Proceedings of the
46th IEEE Conference on Decision and Control
New Orleans, LA, USA, Dec. 12-14, 2007

Performance Analyses of Building Suspension Control with Inerters

Fu-Cheng Wang, Cheng-Wei Chen, Min-Kai Liao and Min-Feng Hong

***Abstract*—This paper discusses the application of a new mechanical element, called Inerter, to building suspension control. The inerter was proposed as a real two-terminal mechanical element, which is a substitute for the mass element, with the applied force proportional to the relative acceleration across two terminals. To investigate the performance benefits of building suspension with inerters, three building models were utilized to analyze the performance using two proposed performance indices. From the simulation results, inerters were deemed effective in reducing vibrations from earthquakes and traffic.**

I. Introduction

THE vibration control of buildings can be mainly divided into two categories, namely the resistant structure and the isolated structure. The former utilizes the elastic properties of buildings to sustain or absorb vibration energy, such as earthquakes [1]. The latter applies isolators at the bases of buildings in order to suppress the input energy by specifying the resonance frequencies [2]. Two passive elements, namely rubber isolators and steel springs, are frequently adopted in the current applications. Alder and Fuller [3] verified the elastic properties of rubber isolators, and discussed their design and implementation. Waller [4] investigated steel springs to cope with traffic vibration. Kelly [5] reviewed the proposed structures which decoupled the damaging effects of ground movements. Clough and Penzien [6] utilized Dynamic-Stiffness matrices to explain the resonance phenomena. Chua et al. [7] and Thornely-Taylor [8] applied finite-element and finite-difference methods, respectively, to analyze two-dimensional beam structures and discussed the influence of element numbers. Talbot and Hunt [9] proposed Insertion Gain and Power Flow Insertion Gain to evaluate the performance of building isolation. In this paper, we propose two performance indices to discuss the performance benefits of building suspension employing inerters. Three building models, namely the rigid-body, flexible column and portable frame models, are utilized to discuss the parameter optimization and corresponding responses.

The inerter was recently proposed as an ideal two-terminal mechanical element to substitute for the mass element, with the applied force proportional to the relative acceleration across two terminals. Ideal inerters have been applied to vehicle, motorcycle and train suspension control [10, 11, 12], where significant performance improvement was noticed. In [13], the Inerter nonlinearities and their impact on system performance were investigated. In this paper, we explore the application of inerters to building suspension control. It is arranged as follows: in section II, a rigid-body building model is considered for performance analysis. We propose two measures to discuss the performance improvement by suspension struts with inerters. In section III, the ideas are extended by considering a flexible-column model of buildings. In section IV, a portal frame building model is established to analyze the system performance. Finally, we draw some conclusions in section V.

II. The Rigid-Body Model

In modeling the building as a rigid body with two degrees of freedom (DOF), as shown in Figure 1 [9], where Q_i represents the suspension arrangements, the dynamics of the system can be represented as

$$\begin{bmatrix} Ms^2+2Q_b & 0 & 0 \\ 0 & Ms^2+2Q_s & -2HQ_s \\ 0 & -2HQ_s & 2Is^2+H^2Q_s+W^2Q_b \end{bmatrix} \begin{bmatrix} y_v \\ y_h \\ \theta \end{bmatrix} = \begin{bmatrix} 2Q_b & 0 \\ 0 & 2Q_s \\ 0 & -2HQ_s \end{bmatrix} \begin{bmatrix} x_v \\ x_h \end{bmatrix}, \quad (1)$$

where M and I are the mass and inertial of the building, while x_h and x_v are the horizontal and vertical displacements of the building base, and y_h, y_v and θ represent the horizontal, vertical and rotational displacements of the building.

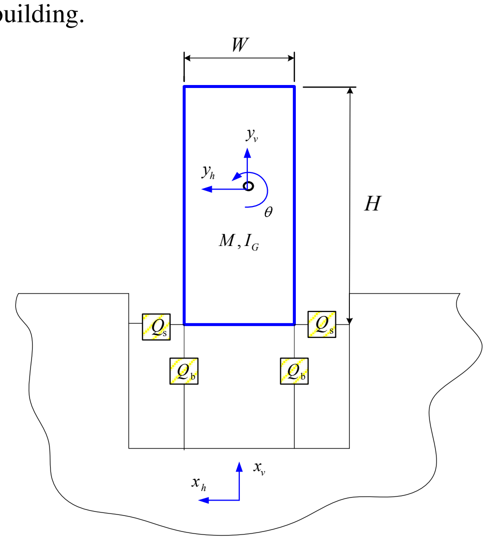

Figure 1. A two-DOF rigid-body model. [9]

Three suspension arrangements, as illustrated in Table 1, are considered to discuss the performance benefits of inerters. It is

Manuscript received on February 28, 2007, and revised on 8th of August. This work was supported in part by the National Science Council of Taiwan under Grant 95-2218-E-002-030.

Fu-Cheng Wang is with the Mechanical Engineering Department of National Taiwan University, No.1, Sec. 4, Roosevelt Road, Taipei 10617, Taiwan. (phone: +886-2-33662680; fax: +886-2-23631755; e-mail: fcw@ntu.edu.tw).

Cheng-Wei Chen, Min-Kai Liao and Min-Feng Hong are all with the Mechanical Engineering Department of National Taiwan University, No.1, Sec. 4, Roosevelt Road, Taipei 10617, Taiwan. (e-mail: r93522827@ntu.edu.tw, r95522816@ntu.edu.tw and r96522806@ntu.edu.tw, respectively).

noted that S2 is a basic parallel arrangement and S3 is a basic serial arrangement.

Table 1. Three suspension models.

S1	S2	S3
$Q_i(j\omega) = jc\omega + k$	$Q_i(j\omega) = -b\omega^2 + jc\omega + k$	$Q_i(j\omega) = k + \left(\frac{1}{jc\omega} - \frac{1}{b\omega^2}\right)^{-1}$
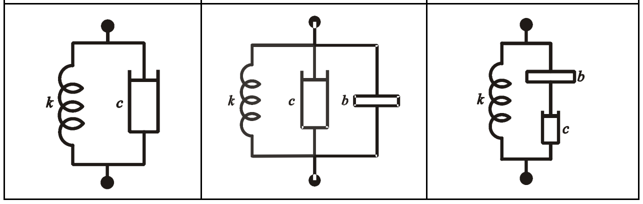		

To discuss the performance, we consider the Insertion Gain (IG) of the system as [14]:

$$\mathrm{IG}_i = \frac{y_i}{x_i}, \quad (2)$$

where $i = h$ (or $i = v$) represents the frequency responses and performance in the horizontal (or vertical) directions. It is noted from (1) that the dynamics in the horizontal and rotational directions are coupled. Therefore, we can evaluate the system performance in the vertical and horizontal directions. Two performance indices J_∞ and J_2 are proposed as follows:

$$J_{\infty,\, i} = \sup_{\omega \in [\omega_1, \omega_2]} \left|\mathrm{IG}_i(\omega)\right|, \quad (3)$$

$$J_{2,\, i} = \sqrt{\int_{\omega_1}^{\omega_2} \left|\mathrm{IG}_i(\omega)\right|^2 d\omega}, \quad (4)$$

in which $\omega \in [\omega_1, \ \omega_2]$ are the concerned frequency range. The indices are so chosen since the H_∞ norm of the system equals to the supreme ratio of the output 2-norm to the input 2-norm, while the H_2 norm of the system indicates the maximum ratio of the output ∞-norm to the input 2-norm [15]. That is, they indicate the supreme (worst) outputs in terms of energy or the absolute magnitude corresponded to a fixed input. Considering the disturbance sources, the frequencies are set as $\omega \in [0.5, \ 10]$ Hz for the primary earthquake and $\omega \in [5, \ 25]$ Hz for the traffic factor (wheel-passing) [16].

The following parameters are used for simulations: *H*=50m, *W*=20m, $M = 10^6$ kg. The suspension stiffness is set as $k = 10^5$ - 10^8 N/m and the resonance frequency of the building is set between 0.05 Hz and 1.59 Hz [17]. To optimize the performance measures, the damping rates (*c's*) and the inertance (*b's*) are tuned to achieve the smallest values of J_2 and J_∞ at each fixed stiffness settings (*k's*).

A. Vertical Direction

The optimization of $J_{\infty,\, v}$ is illustrated in Figure 2, where S2 achieves significant performance improvement for the traffic factor, while S3 is slightly better than S2 for earthquakes. Considering specific stiffness settings $k = 10^8$ N/m for the traffic factor and $k = 1.1 \times 10^7$ N/m for the earthquake, the optimal parameter settings are illustrated in Table 2, where the S2 (S3) layout achieves 55% (58%) for the traffic factor (earthquake). The corresponding Bode plots of these models are shown in Figure 3, where the notches are noted to be beneficial in improving the performance.

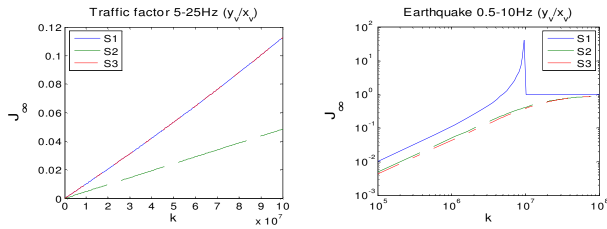

(a) For traffic factor. (b) For earthquake.

Figure 2. Optimization of $J_{\infty,\, v}$.

TABLE 2. J_∞ OPTIMIZATION ON THE VERTICAL DIRECTION.
(*b* in the unit of kg, *c* in the unit of Ns/m)

layout	Traffic factor ($k = 10^8$ N/M)	Earthquake ($k = 1.1\times10^7$ N/M)
S1	J_∞ =0.1127, c =0	J_∞ =1, $c = \infty$
S2	$J_\infty = 0.0485$ b =55047, c =0, 57% Improvement	$J_\infty = 0.4494$ $b = 8.19\times10^5$, c =0, 55% Improvement
S3	J_∞ =0.1127 b =11034, c =0, 0% Improvement	$J_\infty = 0.4219$ $b = 8.98\times10^5$, $c = 1.39\times10^7$, 58% Improvement

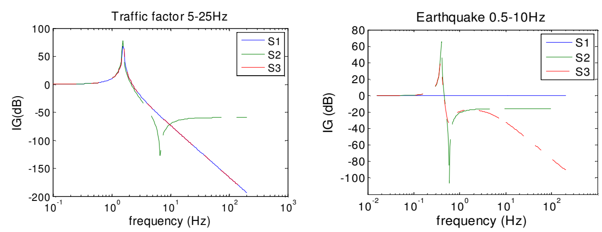

(a) For traffic factor. (b) For earthquake.

Figure 3. Bode plots with the optimal settings for $J_{\infty,\, v}$.

The optimization of $J_{2,\, v}$ is illustrated in Figure 4, where S2 achieves about 29% performance improvement for the traffic factor at all stiffness settings, while S3 is a better choice for the earthquake. Setting the stiffness $k = 10^8$ N/m for the traffic effect ($k = 1.1\times10^7$ N/m for earthquake), the optimal Bode plots are shown in Figure 5, where the S2 (S3) achieves 30% (37%) improvement.

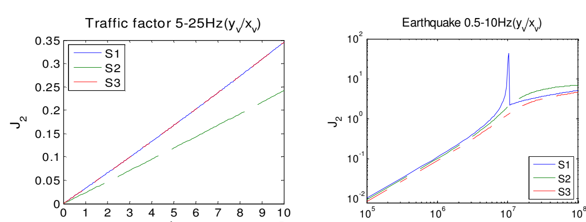

(a) For traffic factor. (b) For earthquake.

Figure 4. Optimization of $J_{2,\, v}$.

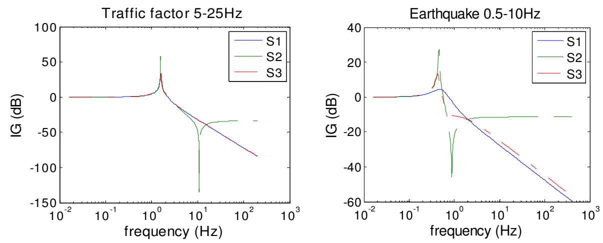

(a) For traffic factor. (b) For earthquake.

Figure 5. Bode plots with the optimal settings for $J_{2,v}$.

B. Horizontal Direction

The optimization of $J_{\infty,h}$ is shown in Figure 6, where S3 is better for both the traffic vibration and earthquake, with performance improvement of about 100% and 75%, respectively. On the other hand, S2 achieves about 81% performance improvement for traffic vibration when $k \geq 10^6$ N/m.

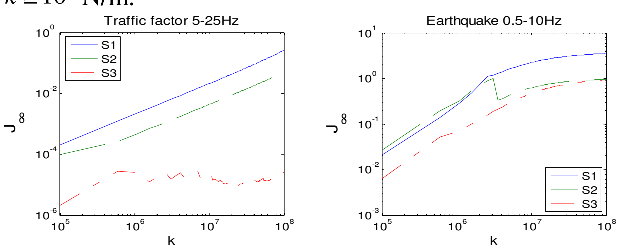

(a) For traffic factor. (b) For earthquake.

Figure 6. Optimization of $J_{\infty,h}$.

Figure 7 shows optimization of $J_{2,h}$, where S3 is the best for both the earthquake and traffic vibrations, with nearly 100% improvement for all stiffness settings.

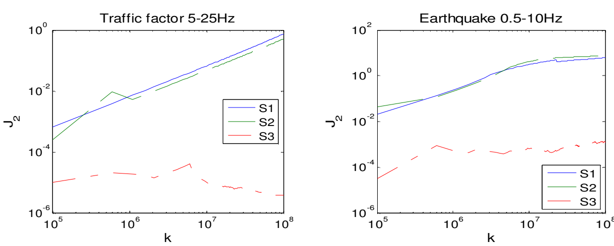

(a) For traffic factor. (b) For earthquake.

Figure 7. Optimization of $J_{2,h}$.

C. Multilayer Design

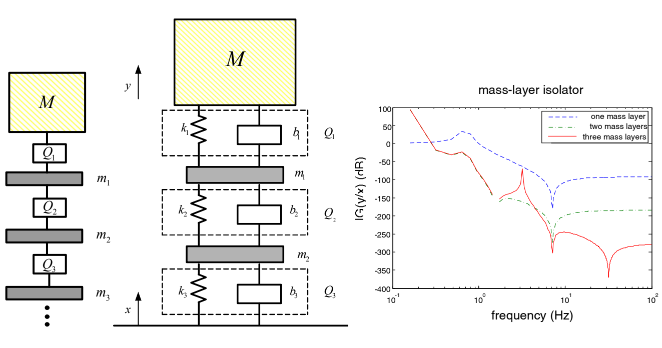

(a) N-layers. (b) Two-layers. (c) Bode plots.

Figure 8. Multi-layer suspension design.

From the discussion in II.*A* and II.*B*, it is noted that applying inerters to the suspension design introduces notches on the Bode plots, which is beneficial in reducing the performance indices. Besides, we also observed that adding dampers tends to have little effect on the performance optimizations. Therefore, in this section multi-layer suspensions are proposed to the building base to discuss the performance improvements.

A multi-layer building suspension is shown in Figure 8(a). Suppose the masses between each layers are $m_1 \cdots m_N$, the IG of the system on the vertical direction can be expressed as

$$\mathrm{IG_N}\left(\frac{y}{x}\right)=\frac{Q_1Q_2\cdots Q_{N+1}}{\left(Ms^2+Q_1\right)\left(m_1s^2+Q_2\right)\cdots\left(m_Ns^2+Q_{N+1}\right)}. \quad (5)$$

Suppose the suspension Q_i is a parallel combination of spring k_i and inerter b_i, (5) can be further simplified by $Q_N = k_N + b_N s^2$. For example, suppose N=2, the suspension arrangement is illustrated in Figure 8(b). Given $M=10^6$ kg, $k_1=k_2=k_3=10^6$ N/m, $m_1=0.05M$, $m_2=0.05m_1$, $b_1=0.01m_1$, $b_2=0.01m_2$, $b_3=0.01m_3$, the Bode plots are shown in Figure 8(c), where the multi-layer design can potentially reduce the responses.

III. Flexible Column Model

The aforementioned rigid-body model provides some intuitions on the suspension design of buildings. However, the elastic effects of buildings are ignored by the simplification. Therefore, in this section we consider the flexible column model, and discuss the suspension benefits of inerters.

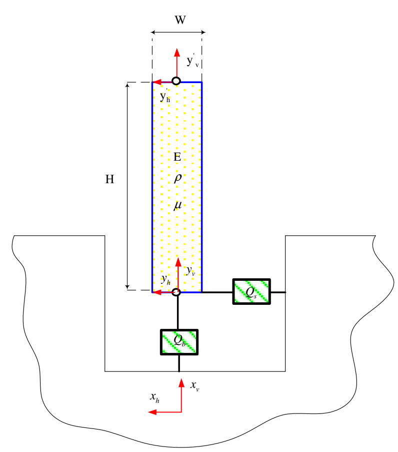

Figure 9. The flexible column model. [17]

A flexible column model of building is illustrated in Figure 9 [17], in which x_h and x_v are the horizontal and vertical disturbance inputs, while y_h and y_v are the horizontal and vertical displacements on the base of the building, and $y_h^{'}$ and $y_v^{'}$ are the horizontal and vertical displacements on the top of the building. The base isolator and side isolator are represented by Q_b and Q_s. The dynamic equations of the model are as follows [18]:

$$IG\left(\frac{y_v}{x_v}\right) = \left| Q_b / \left(\frac{EA\lambda}{\coth(\lambda H)} + Q_b \right) \right|, \quad (6)$$

$$IG\left(\frac{y_h}{x_h}\right) = \left| Q_s / \left(\frac{EA\lambda}{\coth(\lambda W)} + Q_s \right) \right|, \quad (7)$$

$$IG\left(\frac{y'_v}{x_v}\right) = IG\left(\frac{y_v}{x_v}\right) + \left| \frac{2}{e^{\lambda H} + e^{-\lambda H}} \right|, \quad (8)$$

$$IG\left(\frac{y'_h}{x_h}\right) = IG\left(\frac{y_h}{x_h}\right) + \left| \frac{2}{e^{\lambda W} + e^{-\lambda W}} \right|, \quad (9)$$

in which

$$\lambda = \left[\left(\frac{\rho\omega^2}{E} \right)^2 + \left(\frac{\mu\omega}{E} \right)^2 \right]^{\frac{1}{4}} \left(\sin\frac{\theta}{2} + i\cos\frac{\theta}{2} \right), \ \theta = \tan^{-1}\left(\frac{\mu}{\rho\omega} \right).$$

From (6-9), it is noted that the performance on the top is directly related to the performance on the base. Therefore, we will only discuss the performance on the base, using the definition of (2-3). Note that $J_{\infty,v}$ and $J_{\infty,h}$ represent the optimization of J_∞ using the base and the side isolators, respectively, while $J_{2,v}$ and $J_{2,h}$ stand for the optimization of J_2. With the parameter settings of Table 3, the optimization for the three suspension layouts is carried out by fixing the stiffness. The optimization of J_∞ using the base isolator and side isolator is illustrated in Figure 10, where the layout S3 is always the best.

Table 3. Parameter settings for the flexible column model.

Symbol	value
Young's modulus of elements (E)	10×10^9 N/m^2
Cross-sectional area (A)	2.5 m^2
Density of elements (ρ)	2400 kg/m^3
Viscous damping coefficient per unit area ($\mu = c/A$)	5.13×10^4 Ns/m^4
Height of building (H)	30 m
Weight of building (W)	3 m

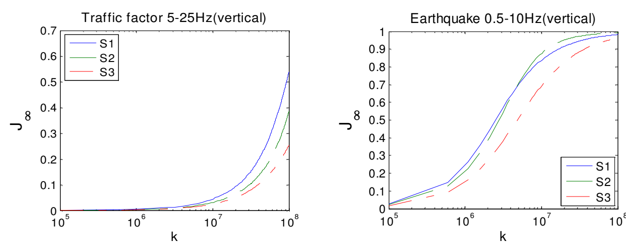

(a) $J_{\infty,v}$ for traffic factor. (b) $J_{\infty,v}$ for earthquake.

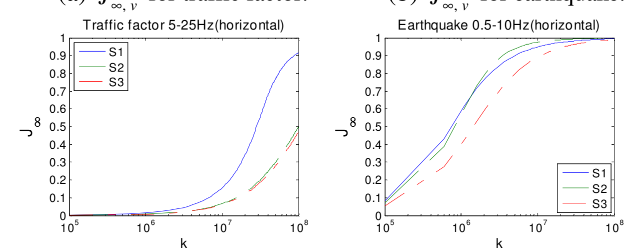

(c) $J_{\infty,h}$ for traffic factor. (d) $J_{\infty,h}$ for earthquake.

Figure 10. Optimization of J_∞ for the flexible column model.

Similarly, the optimization of J_2 is shown in Figure 11, where the S3 layout is always the best.

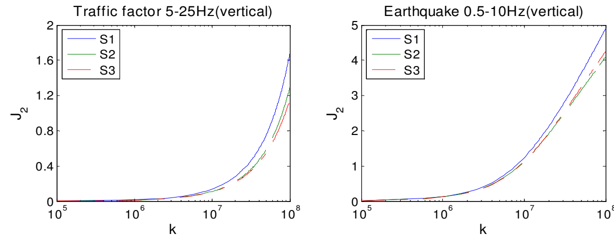

(a) $J_{2,v}$ for traffic factor. (b) $J_{2,v}$ for earthquake.

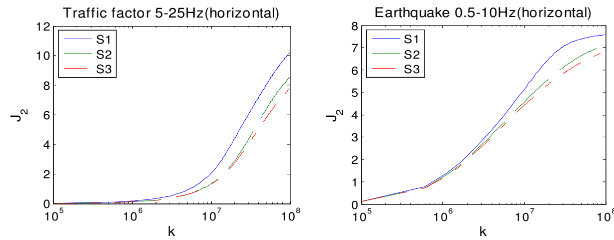

(c) $J_{2,h}$ for traffic factor. (d) $J_{2,h}$ for earthquake.

Figure 11. Optimization of J_2 for the flexible column model.

IV. Portal Frame Model

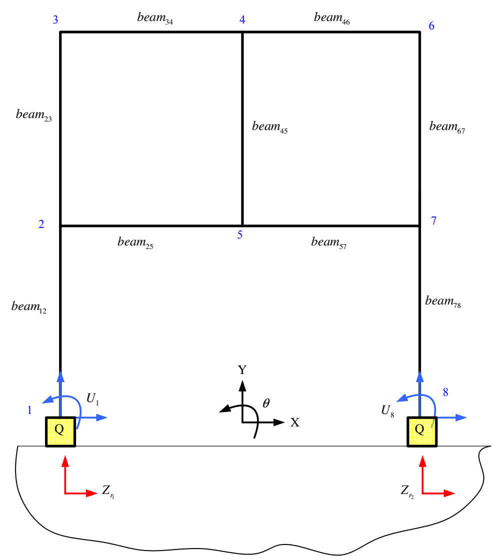

Figure 12. A portal frame model.

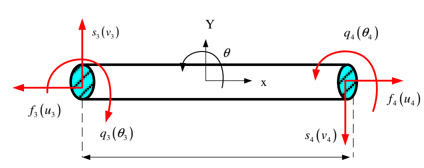

Figure 13. Free-body diagram of $beam_{34}$. [17]

The portal-frame model, as shown in Figure 12 [17], is frequently used for the analyses of modern buildings, where the floors and walls are represented by elastic beams. Isolators are located at the base of the building. Each beam has two joints, which are connected to other beams. Each joint has three DOF, in the translational, lateral and rotational directions. Therefore, there are twenty-four DOF for the model of Figure 12. To discuss the coupling effects of the structures, we firstly analyze the free-body diagram of $beam_{34}$, as illustrated in Figure 13. Suppose the translation, lateral and rotational displacements of joint 3 (joint 4) are labeled as u_3, v_3 and θ_3 (u_4 , v_4 and θ_4), and the forces/moments on these directions are labeled as f_3, s_3 and q_3 (f_4, s_4 and q_4), then the dynamics of $beam_{34}$ can be represented as follows [17]:

$$\begin{bmatrix} F_3 \\ F_4 \end{bmatrix} = K_{34} \begin{bmatrix} U_3 \\ U_4 \end{bmatrix} \tag{10}$$

in which

$$K_{34} = \begin{bmatrix} -AE\alpha e^{-\frac{\alpha L}{2}} & AE\alpha e^{\frac{\alpha L}{2}} & 0 & 0 & 0 & 0 \\ 0 & 0 & EI\beta^3 e^{\frac{-\beta L}{2}} & -iEI\beta^3 e^{\frac{-i\beta L}{2}} & -EI\beta^3 e^{\frac{\beta L}{2}} & iEI\beta^3 e^{\frac{i\beta L}{2}} \\ 0 & 0 & -EI\beta^2 e^{\frac{-\beta L}{2}} & EI\beta^2 e^{\frac{-i\beta L}{2}} & -EI\beta^2 e^{\frac{\beta L}{2}} & EI\beta^2 e^{\frac{i\beta L}{2}} \\ AE\alpha e^{\frac{\alpha L}{2}} & -AE\alpha e^{\frac{-\alpha L}{2}} & 0 & 0 & 0 & 0 \\ 0 & 0 & -EI\beta^3 e^{\frac{\beta L}{2}} & iEI\beta^3 e^{\frac{i\beta L}{2}} & EI\beta^3 e^{\frac{-\beta L}{2}} & -iEI\beta^3 e^{\frac{-i\beta L}{2}} \\ 0 & 0 & EI\beta^2 e^{\frac{\beta L}{2}} & -EI\beta^2 e^{\frac{i\beta L}{2}} & EI\beta^2 e^{\frac{-\beta L}{2}} & -EI\beta^2 e^{\frac{-i\beta L}{2}} \end{bmatrix}$$

$$\bullet \begin{bmatrix} e^{-\frac{\alpha L}{2}} & e^{\frac{\alpha L}{2}} & 0 & 0 & 0 & 0 \\ 0 & 0 & e^{\frac{-\beta L}{2}} & e^{\frac{-i\beta L}{2}} & e^{\frac{\beta L}{2}} & e^{\frac{i\beta L}{2}} \\ 0 & 0 & \beta e^{\frac{-\beta L}{2}} & i\beta e^{\frac{-i\beta L}{2}} & -\beta e^{\frac{\beta L}{2}} & -i\beta e^{\frac{i\beta L}{2}} \\ e^{\frac{\alpha L}{2}} & e^{\frac{-\alpha L}{2}} & 0 & 0 & 0 & 0 \\ 0 & 0 & e^{\frac{\beta L}{2}} & e^{\frac{i\beta L}{2}} & e^{\frac{-\beta L}{2}} & e^{\frac{-i\beta L}{2}} \\ 0 & 0 & \beta e^{\frac{\beta L}{2}} & i\beta e^{\frac{i\beta L}{2}} & -\beta e^{\frac{-\beta L}{2}} & -i\beta e^{\frac{-i\beta L}{2}} \end{bmatrix}^{-1}, \quad F_i = \begin{bmatrix} f_i \\ s_i \\ q_i \end{bmatrix}, \quad U_j = \begin{bmatrix} u_j \\ v_j \\ \theta_j \end{bmatrix}$$

and

$$\beta = \left(\frac{\rho A \omega^2}{EI} \right)^{\frac{1}{4}}, \quad \alpha = \omega \sqrt{\frac{\rho}{E}} . \tag{11}$$

Considering the rotation of other beams, the complete dynamic equations of the system can be represented as:

$$[\Sigma F]_{24\times1} = [K]_{24\times24} [U]_{24\times1}, \tag{12}$$

in which

$$K = \begin{bmatrix} K_{12}^{11} & 0 & K_{12}^{12} & 0 & 0 & 0 & 0 & 0 \\ 0 & K_{78}^{22} & 0 & 0 & 0 & 0 & 0 & K_{78}^{21} \\ K_{12}^{21} & 0 & K_{12}^{22}+K_{23}^{11}+K_{25}^{11} & K_{23}^{12} & 0 & K_{25}^{12} & 0 & 0 \\ 0 & 0 & K_{23}^{21} & K_{23}^{22}+K_{34}^{11} & K_{34}^{12} & 0 & 0 & 0 \\ 0 & 0 & 0 & K_{34}^{21} & K_{34}^{22}+K_{46}^{11}+K_{45}^{11} & K_{45}^{12} & K_{46}^{12} & 0 \\ 0 & 0 & K_{25}^{21} & 0 & K_{45}^{21} & K_{45}^{22}+K_{25}^{22}+K_{57}^{11} & 0 & K_{57}^{12} \\ 0 & 0 & 0 & 0 & K_{46}^{21} & 0 & K_{46}^{22}+K_{67}^{11} & K_{67}^{12} \\ 0 & K_{78}^{12} & 0 & 0 & 0 & K_{57}^{21} & K_{67}^{21} & K_{67}^{22}+K_{78}^{11}+K_{57}^{22} \end{bmatrix}_{24\times24}$$

$$U = \begin{bmatrix} U_b \\ U_s \end{bmatrix}, \quad \Sigma F = \begin{bmatrix} F_b \\ \Sigma F_s \end{bmatrix},$$

where the subscripts "$_b$" and "$_s$" represent "base" and "structure", respectively. That is,

$$U_b = \begin{bmatrix} U_1 \\ U_8 \end{bmatrix}_{6\times1}, \quad U_s = \begin{bmatrix} U_1 \\ \vdots \\ U_7 \end{bmatrix}_{18\times1}, \quad F_b = \begin{bmatrix} F_1 \\ F_8 \end{bmatrix}_{6\times1}, \quad \Sigma F_s = \begin{bmatrix} \Sigma F_2 \\ \vdots \\ \Sigma F_7 \end{bmatrix}_{18\times1}$$

in which ΣF_i represents the resultant force acting on joint *i*.

Suppose the road inputs on joints 1 and 8 are z_{r_1} and z_{r_2} with suspension Q_1 and Q_2, the forces acting on the joints are:

$$F_b = \begin{bmatrix} F_1 \\ F_8 \end{bmatrix}_{6\times1} = \begin{bmatrix} Q_1 (U_1 - Z_{r_1}) \\ Q_2 (U_8 - Z_{r_2}) \end{bmatrix}_{6\times1} \tag{13}$$

To simplify the expression of (12), we define $H = K^{-1}$ and partition (12) conformally as:

$$\begin{bmatrix} U_b \\ U_s \end{bmatrix}_{24\times1} = \begin{bmatrix} [H^{11}]_{6\times6} & [H^{12}]_{6\times18} \\ [H^{21}]_{18\times6} & [H^{22}]_{18\times18} \end{bmatrix}_{24\times24} \begin{bmatrix} F_b \\ \Sigma F_s \end{bmatrix}_{24\times1} . \tag{14}$$

If we ignore the weights of joints, the resultant forces acting on each joint of structures equal to zero, i.e. $\Sigma F_s = 0$ and (14) is simplified as:

$$[U]_{24\times1} = \begin{bmatrix} H^{11} \\ H^{21} \end{bmatrix}_{24\times6} [F_b]_{6\times1} = [H_s][F_b]_{6\times1} \tag{15}$$

Combining (13) with (15), the displacements of all joints can be evaluated from the inputs z_{r_1} and z_{r_2}:

$$[U]_{24\times1} = \left([I]_{24\times24} - [H_s]_{24\times6} [R]_{6\times24}\right)^{-1} [H_s]_{24\times6} [P]_{6\times6} [Z_r]_{6\times1}, \tag{16}$$

in which

$$R = [P_{6\times6} \quad 0_{6\times18}], \quad P = \begin{bmatrix} [Q_1]_{3\times3} & 0 \\ 0 & [Q_2]_{3\times3} \end{bmatrix}_{6\times6}, \quad Z_r = \begin{bmatrix} Z_{r_1} \\ Z_{r_2} \end{bmatrix}_{6\times1} .$$

Since the model of (16) is much more complicated than the previous rigid-body or flexible beam models, in order to analyze the performance, we consider the Power Flow Insertion Gain (PFIG) defined as follows [19]:

$$\text{PFIG} = \frac{P_{isol}}{P_{unisol}}, \tag{17}$$

where P_{unisol} and P_{isol} represent the instant power of the structure without and with isolators, respectively, which are defined as:

$$P = \frac{-1}{2} \text{Re}\left\{ i\omega \left(uf^* + vs^* + \theta q^* \right) \right\} .$$

We then defined the performance indices J_∞ and J_2 of the system as follows:

$$J_\infty = \sup_{\omega \in [\omega_1, \omega_2]} \left| \text{PFIG}(\omega) \right|, \tag{18}$$

$$J_2 = \sqrt{\int_{\omega_1}^{\omega_2} \left| \text{PFIG}(\omega) \right|^2 d\omega}, \tag{19}$$

in which $\omega \in [\omega_1, \ \omega_2]$ are the concerned frequency range. We carried out the performance analyses using the following parameters [17]: Young's modulus of the elements $E=10\times10^9$ N/m^2, cross-sectional area $A=0.25\pi$ m^2, density of elements $\rho=2400$ kg/m^3, damping loss factor $\eta=0.1$ and length of elements L=10 m.

The optimization of J_∞ is illustrated in Figure 14. For the traffic factor, S2 can improve 100% of the performance for nearly all stiffness settings, as illustrated in Figure 14(a). As for earthquakes, both S2 and S3 achieve about 100% improvement for all stiffness settings (except when $k = 10^8 \sim 10^9$ N/m), as shown in Figure 14(b). Setting the stiffness $k = 5\times10^9$ N/m, the corresponding Bode plots using optimal parameters are illustrated in Figure 14(c)(d).

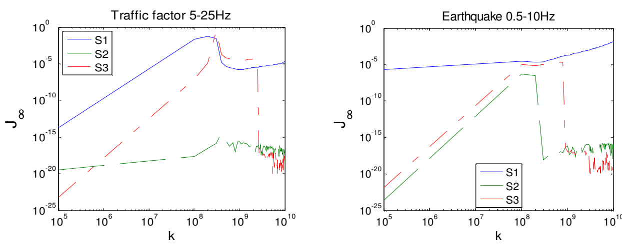

(a) for traffic factor. (b) for earthquake.

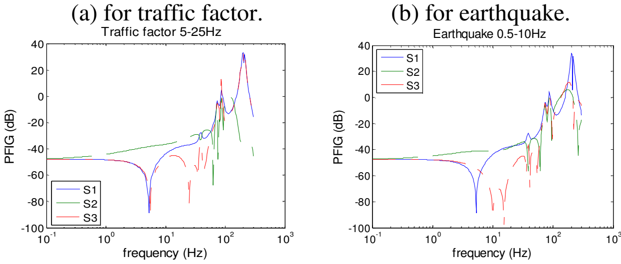

(c) $k = 5\times10^9$ N/m (traffic). (d) $k = 5\times10^9$ N/m (earthquake).

Figure 14. Optimization of J_∞ using the portal frame model.

The optimization of J_2 is shown in Figure 15. For the traffic factor, using inerters is not very beneficial in improving performance, as seen in Figure 15(a). On the other hand, the performance improvement for earthquake is mainly at low stiffness settings, as illustrated in Figure 15(b). Setting the stiffness $k = 1.1\times10^9$ for the traffic factor and $k = 5.1\times10^8$ N/m for earthquakes, the corresponding Bode plots using optimal parameter settings are illustrated in Figure 15(c)(d).

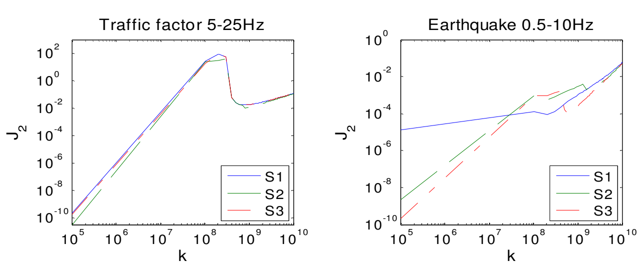

(a) for traffic factor. (b) for earthquake.

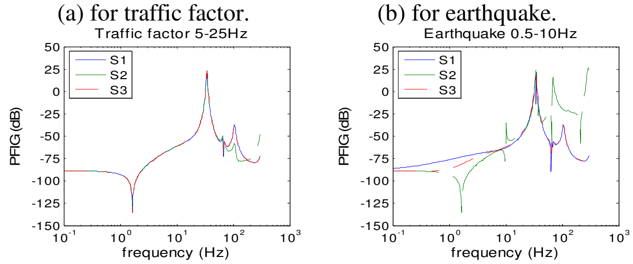

(c) $k = 1.1\times10^9$ N/m (traffic). (d) $k = 5.1\times10^8$ N/m(earthquake).

Figure 15. Optimization of J_2 using the portal frame model.

V. Conclusion

This paper has discussed the performance benefits of building suspension design employing inerters. Three building models, namely the rigid-body, flexible beam and portal frame models, were considered for the performance analyses. Three basic suspension layouts were introduced for numerical optimization. From the simulation results, inerters were deemed effective in suppressing vibrations from both traffic and earthquake vibrations. Further studies can be carried out by considering complicated suspension layouts or LMI approaches, as illustrated in [20].

References

[1] M. Paz, *Structural Dynamics: theory and Computation*, 4th Ed., Earthquake Engineering Research Institute, Berkeley,1982.

[2] R.L. Mayes, *Design of Structures with Seismic Isolation, The Seismic Design Handbook*, Edited by Naeim, F.,1989.

[3] A.J. Alder and K.N.G. Fuller, *Elastonmeric isolation mounts for buildings and structures: from design to installation*. Proceedings of the Institute of Acoustics, 1999, 21(3), pp.17-25.

[4] R.A. Waller, *Building on Springs*. Pergamon Press,1969

[5] J.M. Kelly, *A seismic base isolation: review and bibliography*, Soil Dynamics and Earthquake Engineering, 5, No.3, 1986, pp.202-216.

[6] R.W. Clough and J. Penzien, *Dynamics of Structures*, Second Ed., McGraw-Hall ,New York,1993.

[7] K.H. Chua et al., *Building response due to subway train traffic*. Journal of Geotechnical Engineering, American Society of civic Engineers, Nov. 1995, pp.747-754.

[8] R.M. Thornely-Taylor, *Modeling of vibration and ground-borne noise from underground railway tunnels by a finite difference method.* Proceedings of the 6th International Congress on Sound and Vibration, Copenhagen, Denmark, 1999. International Institute of Acoustics and Vibration.

[9] J.P. Talbot, and H.E.M. Hunt, *The effect of side-restraint bearings on the performance of base-isolated buildings*, Proc I Mech. E. 2003 Part C 217, 849-859.

[10] M.C. Smith, and F.C. Wang, *Performance Benefits in Passive Vehicle Suspensions Employing Inerters.* Vehicle System Dynamics 42 (4): 235-257 OCT 2004.

[11] S. Evangelou, D.J.N. Limebeer, R.S. Sharp and M.C. Smith, *Steering Compensation for High-Performance Motorcycles*, Proceedings of the 43rd IEEE Conference on Decision and Control, Paradise Island, Bahamas, 14-17 December, 2004, pp. 749–754.

[12] F.C. Wang, et al. *The Performance Improvements of Train Suspension Systems with Inerters*, Proceedings of the 45th IEEE Conference on Decision and Control, pp. 1472-1477, San Diego, CA, USA December, 2007.

[13] F.C. Wang and W.J. Su, *The Impact of Inerter Nonlinearities on Vehicle Suspension Control*, accepted, to appear in Vehicle System Dynamics.

[14] A.K. Sharif, *Dynamic performance investigation of base -isolated structures*. Ph.D. dissertation, Imperial College of Science, Technology and Medicine, 1999.

[15] J.C. Doyle, B.A. Francis and A.R. Tannenbaum, *Feedback Control Theory*, Maxwell Macmillan, 1992.

[16] H. Hao, et al., *Building vibration to traffic-induced ground motion*. Building and Environment, 2001, 36, pp321-336.

[17] J.P. Talbot and H.E.M. Hunt, *A generic model for evaluating the performance of base-isolated buildings*, J. Low Frequency Noise , Vibration and Active Control,2003, Vol. 22(3) 149-160

[18] D.E. Newland, *Mechanical Vibration Analysis and Computation*. Longman, 1989.

[19] R.S. Langley, *Analysis of power flow in beams and frameworks using the direct-dynamic stiffness method*. Journal of Sound and Vibration, 1990, 136(3), pp.439-452.

[20] C. Papageorgiou and M.C. Smith, *Positive Real Synthesis Using Matrix Inequalities for Mechanical Networks: Application to Vehicle Suspension*, IEEE Trans. on Contr. Syst. Tech. 14 (2006), pp. 423–435.